

# Compact Integrated Silicon Photonic Mems Power Coupler for Programmable Photonics

Alain Yuji Takabayashi<sup>1</sup>, Duarte Silva<sup>1</sup>, Hamed Sattari<sup>1</sup>, Pierre Edinger<sup>2</sup>, Peter Verheyen<sup>3</sup>,  
Kristinn B. Gylfason<sup>2</sup>, Wim Bogaerts<sup>4</sup>, Niels Quack<sup>1,5</sup>

<sup>1</sup>Ecole Polytechnique Fédérale de Lausanne (EPFL), SWITZERLAND

<sup>2</sup>KTH Royal Institute of Technology, SWEDEN

<sup>3</sup>Interuniversity Microelectronics Centre (IMEC), BELGIUM

<sup>4</sup>Ghent University-IMEC, BELGIUM

<sup>5</sup>The University of Sydney, AUSTRALIA

## ABSTRACT

Programmable photonics promise a plethora of optical functions while at the same time reducing the time and costs of photonic integrated circuit (PIC) development. One primary bottleneck for development of these systems is the difficulty in increasing component density because of excessive power consumption. We here present a MEMS-based Silicon Photonic power coupler that offers high optical performance ( $> 18$  dB extinction ratio (ER),  $< 1.2$  dB insertion loss (IL), and  $> 80$  nm of optical bandwidth) within a compact footprint ( $25 \mu\text{m} \times 150 \mu\text{m}$ ) to provide a power-efficient active function: fast, continuous power tuning.

## KEYWORDS

Microelectromechanical systems, photonic integrated circuits, silicon photonics, photonics, power coupler.

## INTRODUCTION

The field of integrated photonics has developed over the last few decades in a manner similar to that of integrated electronics. In particular, research has focused on creating smaller, more power-efficient devices that can be densely integrated with one another at large-scale to implement novel and complex circuit functions. These photonic integrated circuits (PICs) find application in, among others, precision metrology and spectroscopy, bio-sensing, tele- and datacom, and quantum computation [1].

Although there are several established and emerging technologies for the implementation of integrated photonics, one material platform naturally lends itself to the fabrication of large-scale integrated PICs: silicon. Silicon has a high refractive index ( $n = 3.47$ ) which allows for tight light confinement, thereby allowing micron-scale bending radii and overall compact devices [2]. Moreover, it is the same material used in the CMOS electronics industry, and therefore benefits from decades of experience and a robust and mature processing infrastructure. Despite being an indirect bandgap material, efforts to include sources and detectors, e.g., through heterogeneous integration of III-V materials on Si, are well underway [3]. Consequently, Silicon Photonics is one of the few technologies capable of providing integrated photonics with the large throughput and cost reduction that drives the electronics industry.

The high refractive index contrast that allows Silicon Photonic devices to be small also makes them particularly sensitive to geometric variations and environmental influences. Consequently, active compensation is required

for as-designed and stable operation. While thermo-optic tuning of the refractive index is the conventional approach to compensation, it is power hungry, with every element consuming  $\approx 1$  mW. With thousands of elements needed in complex circuits, scaling this solution is impossible. Mechanical tuning via the physical movement of material to modify optical interactions between light-guiding structures is also possible. Moreover, generation of the requisite displacements using electrostatic Microelectromechanical Systems (MEMS), makes this approach a low-power alternative that supports continued scaling in component-density.

Silicon Photonic MEMS-enabled devices, however, not only serve in compensatory roles, but can themselves provide independent active functions such as switching, wavelength-selective filtering, and phase shifting [4-6]. These operations represent a subset of fundamental building blocks that can be used to create a variety of linear optical systems, but also specifically, programmable PICs. Much like the Field Programmable Gate Arrays (FPGAs) in electronics, Field Programmable PICs (FP-PICs) provide a large number of devices whose connectivity can be dynamically reconfigured to perform a variety of functions [7]. Such generalized platforms present an opportunity for cost- and time-effective development cycles and improved accessibility to circuit design.

In the pursuit of compact, low-power, MEMS-enabled devices for enhanced integration and functionality in programmable photonics, we here present an in-plane, electrostatically actuated Silicon Photonic power coupler. The device provides continuous, hysteresis-free optical power tuning from 0 to 100% transmission in the output ports, and exhibits symmetric tuning characteristics for its high Extinction Ratio (ER) in both the unactuated and actuated states. Its broadband behavior, low insertion loss and fast rise-/fall-times make it an attractive component for fast and efficient optical power tuning.

## OPERATING PRINCIPLE AND DESIGN

The optical portion of the device consists of a suspended directional coupler with one movable arm and one fixed arm. By attaching an electrostatic comb-drive to the movable arm, the waveguide gap separation in the directional coupler can be made tunable. These components are illustrated in the device visualization in Figure 1.

The device is nestled within an opening in the Back-End-of-Line (BEOL) stack that provides access to the device layer silicon and surrounding filler oxides. It is

surrounded by a silicon rim that provides optical and electrical I/O and has a footprint of  $25\ \mu\text{m} \times 150\ \mu\text{m}$ . Structurally, the device is fabricated in a 220 nm silicon device layer but also includes 150 nm shallow-etched silicon in the anchoring regions and optical transitions. Beneath these anchors and under the fixed-comb, a 2  $\mu\text{m}$  thick buried oxide (BOx) sacrificial layer affixes these structures to the substrate. By design and timed undercut of the BOx, the directional coupler arms and comb-drives are suspended, with one coupler arm and comb-drive pair also being movable.

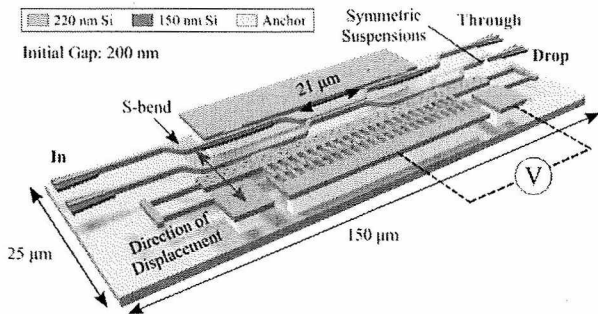


Figure 1: 3D schematic view of the Silicon Photonic MEMS power coupler indicating the optical input and output ports, the direction of displacement, and salient mechanical features such as the S-bends and symmetric suspensions. Layer composition and thicknesses are indicated in the legend and the dimensions, as well the actuation scheme, are also included.

Operationally, the optical power transmission from the input port (In) to the two output ports (Through and Drop) is gap-dependent. The exact relation is modeled by 3D Finite Difference Time Domain (FDTD) simulation of the coupler geometry. A complete discussion of the coupler design and parameters is provided in [8].

As indicated in Figure 1, the coupling region has a physical length of  $21\ \mu\text{m}$ , which in combination with the 200 nm initial gap produces an initial state wherein power is preferentially sent to the Through port. By applying an actuation voltage to the comb-drive, an attractive electrostatic force is generated that pulls the movable arm of the directional coupler away from its fixed counterpart, thereby increasing the gap. This increased waveguide separation causes a reduction in power transmission to the Through port. At a 260 nm gap, power is equally split between the two outputs, and beyond 330 nm, the initial transfer characteristic has been reversed: all the optical power is now in the Drop port.

Key mechanical design features of the device include S-bends and symmetric suspensions for stress-

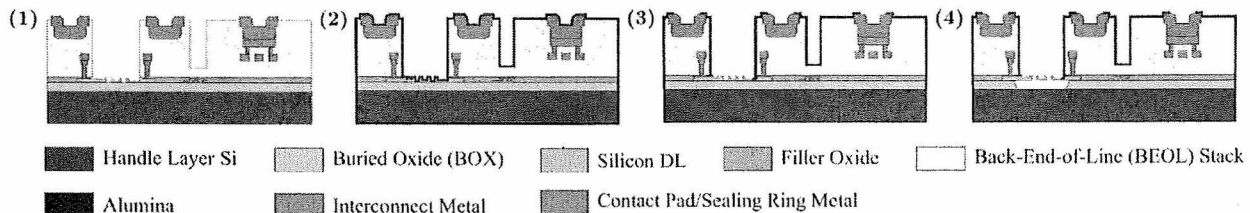


Figure 2: Simplified process flow indicating the four primary steps for producing free-standing movable MEMS (1) Initial sample from silicon photonic foundry (2) Alumina passivation (3) Selective patterning of alumina (4) VHF release step

compensation of residual in-plane stress. Without this preventive mechanism, there is a risk of out-of-plane misalignment in the directional coupler arms after the structure is released from the BOx. This misalignment in turn can lead to a power transfer characteristic different from that which was designed, e.g., an asymmetric ER in the initial, unactuated, and final, actuated states [9]. The use of S-bends in the waveguides also presents a compact compromise between a sufficiently strong out-of-plane stiffness to avoid substrate collapse during release (e.g., stiction) or actuation and a moderate in-plane stiffness to enable sub-20 V actuation voltages in the comb-drive.

## FABRICATION

The sample is designed and fabricated using IMEC's iSiPP50G Silicon Photonics platform, after which it undergoes custom MEMS post-processing at the EPFL's Center of MicroNanoTechnology (CMi). Process development has been performed at coupon- and chip-scale, but all steps are wafer-scale compatible. A short summary of the main steps is provided here and illustrated in Figure 3; for a more complete discussion, please see [10].

Following fabrication and dicing at the foundry, samples undergo a filler oxide removal and subsequent passivation consisting of 50 nm of ALD-deposited alumina. This conformal layer protects regions of the sample, e.g., the Back-End-of-Line (BEOL) stack containing the metallization, from the vapor-phase HF (VHF) that is used to selectively remove the sacrificial BOx layer. The alumina over the contact pads is then removed by a chlorine chemistry based dry etch to ensure proper electrical connections to the electrical probe tips. In a separate step, the alumina within the MEMS cavities is etched using BHF to expose the BOx layer. A final VHF etch is then used to selectively remove the BOx, thereby undercutting the MEMS structures and making them free-standing. A microscope image and an SEM recording of the released device highlighting salient features is presented in Figure 4.

## RESULTS AND DISCUSSION

Following a successful MEMS release, the sample is characterized electrically and optically. Light enters the PIC via a  $1 \times 10$  fiber array that has been connected to a tunable laser and is aligned to a corresponding  $1 \times 10$  grating coupler array on chip. From there, it is routed by the integrated waveguides to the In port and passes through the coupling region of the device. By applying an actuation voltage to the contact pads via a set of probe tips, the comb-

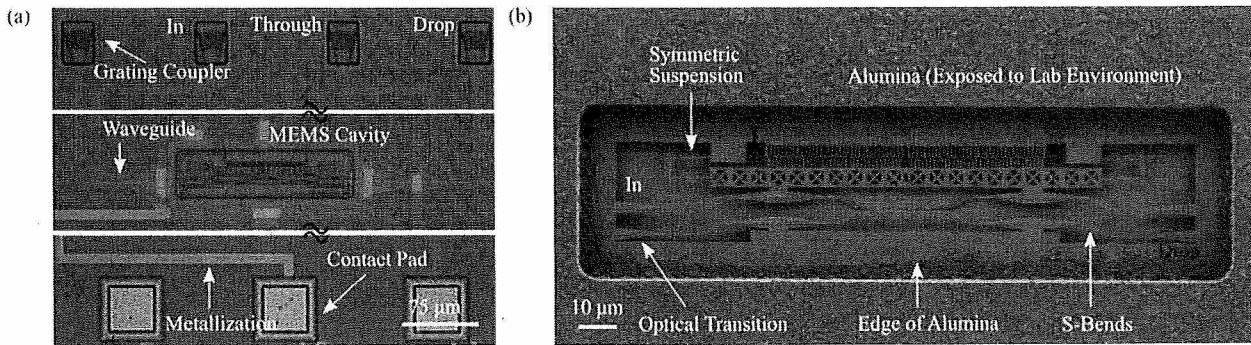


Figure 3: (a) Optical microscope image indicating the device within the MEMS cavity in the BEOL stack; ancillary optical and electrical components such as the grating couplers for optical I/O and contact pads for electrical connections and corresponding routing structures (i.e., waveguides and metal traces) have been indicated (b) SEM recording of the fully characterized power coupler; note that the movable coupler branch collapsed during imaging, but all other portions of the device remain suspended.

drive can be engaged.

In this process, the movable arm of the coupler is pulled away from its fixed counterpart and the gap increases. DC characterization of the device follows this general procedure and involves the measurement of power transmission to the Through and Drop output ports for various actuation voltages. The extracted actuation curve can be seen in Figure 5.

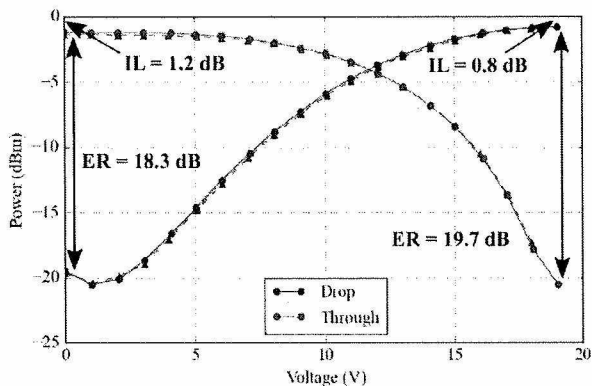


Figure 4: DC actuation characteristics capturing the continuous tuning of optical power transmission wherein light that is initially localized in the Through port (18.3 dB ER) is transferred to the Drop port (19.7 dB ER) at 19 V. Measured data is for  $\lambda = 1540$  nm and 0 dBm input power

As shown in the DC power transmission curve of Figure 5, this power coupler exhibits excellent symmetry in the ER (i.e., > 18 dB) for both the unactuated and actuated states. This favorable property is attributed to a good initial alignment of the directional coupler arms, which is also maintained throughout the actuation of the device. The power coupler can switch power from the Through port to the Drop port after 19 V of actuation voltage, which is not particularly large, but can be further reduced. One strategy would be to increase the length of the symmetric suspensions to reduce in-plane stiffness, but this would come at the cost of a greater susceptibility to out-of-plane collapse. A perhaps better and more elegant solution would be to replace the fixed arm of the directional coupler with another movable one (i.e., mirror the comb-driver along the long-axis). In this manner, the waveguide

gap would be increased from both sides as the two arms are pulled away from one another in opposite directions.

Spectral characterization of the power coupler involves sweeping the wavelength of the light source between 1500 nm and 1580 nm and recording the transmission to the output ports. The result of this characterization is captured in Figure 6. As indicated, the device exhibits respectably broadband behavior with a 3-dB bandwidth exceeding 80 nm covering the entire C-band and more. The relative wavelength-insensitivity of the optical characteristics can be traced back to the tapering at the start of the directional coupler's coupling region from 450 nm to 300 nm [7].

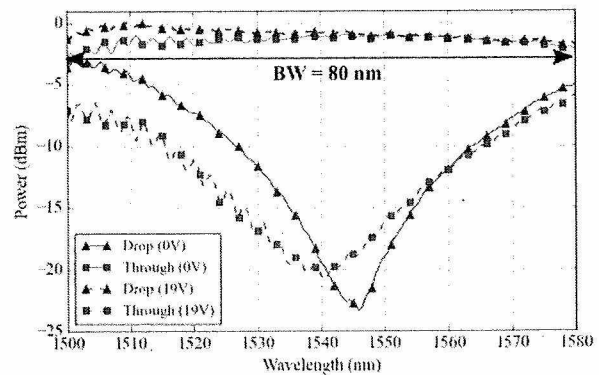


Figure 5: Spectral characterization of the power coupler indicating broadband behavior, > 80 nm 3-dB bandwidth for both the unactuated and actuated states

Following measurement of the power coupler's steady-state behavior, its transient behavior is characterized by replacing the DC actuation voltage with a rectangular pulse. The desired quantity is then the time it takes the output power to switch after the electrical actuation signal has changed. These switching times are observed in the electrical domain through optoelectronic conversion using a high-speed photodetector connected to an oscilloscope. The results for the on/off-switching times are depicted in Figure 7 and indicate a fast response of 15.5  $\mu$ s and 0.8  $\mu$ s, respectively. Although a distinct asymmetry in the switching times can be observed, this is not unexpected because of the non-linear actuation

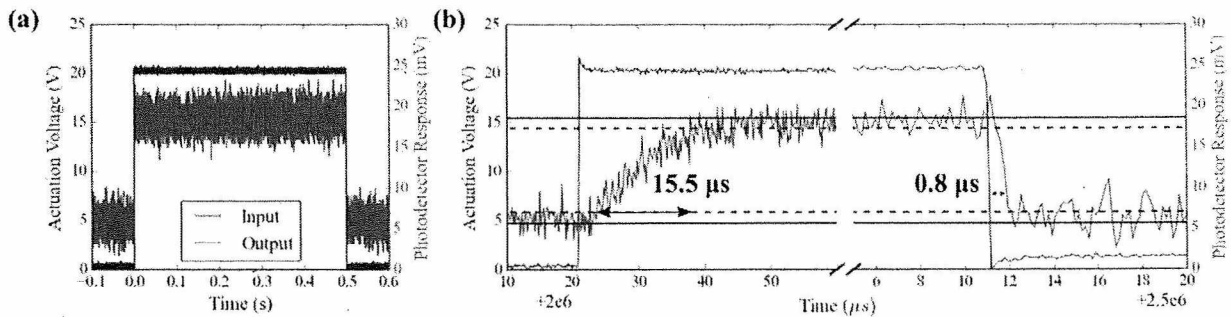


Figure 6: (a) Transient switching time measurement where the actuation voltage is a rectangular pulse and the optical response is measured in the electrical domain through an external, high-speed photodetector and oscilloscope. (b) Close-up for the on-switching showing a  $15.5 \mu\text{s}$  rise-time and for the off-switching showing a  $0.8 \mu\text{s}$  fall-time.

characteristics of the comb-drive. In the unactuated state, there is only a small overlap between the comb-fingers, so the initial force that pulls the waveguides away from one another is small and subsequently, slow. In the fully actuated state, though, the overlap is large and the correspondingly larger electrostatic force is counterbalanced by a large mechanical restoring force from the suspensions. Once the actuation voltage is removed, the electrical force disappears almost instantaneously, leaving the large mechanical force to quickly bring the waveguide back to its initial state. Some ringing after this rapid transition can also be observed in the time following the switching event. Pre-conditioning of the actuator with an offset voltage to increase the initial overlap is expected to reduce the asymmetry.

## CONCLUSION

In this paper, we have presented the design, simulation, fabrication, and measurements of a compact Silicon Photonic MEMS power coupler. The device combines a broadband directional coupler with an in-plane electrostatic actuator to provide continuous optical power tuning between output ports. With a footprint of  $25 \mu\text{m} \times 150 \mu\text{m}$  and 3-dB bandwidth greater than 80 nm, this device reflects equally compact and broadband characteristics. Furthermore, the optical performance of the device in both the unactuated and actuated states ( $> 18 \text{ dB ER}$  and  $< 1.2 \text{ dB IL}$ ) and on-/off-switching times of  $15.5 \mu\text{s}$  and  $0.8 \mu\text{s}$  indicate that this electrical-mechanical-optical modulation is both strong and responsive. Together, these characteristics describe a power coupler well-suited for large-scale integration in programmable photonics that require sub-millisecond reconfiguration times.

## ACKNOWLEDGEMENTS

This project has received funding from the European Union's Horizon 2020 research and innovation program under grant No. 780283 (MORPHIC – [www.h2020morphic.eu](http://www.h2020morphic.eu)). H. Sattari acknowledges funding from the Hasler Foundation under grant No. 17008, and Niels Quack from the Swiss National Science Foundation under grant No. 183717.

## REFERENCES

- [1] D. J. Blumenthal, "Photonic integration for UV to IR applications," *APL Photonics*, vol. 5, p. 020903, Feb. 2020.
- [2] L. Li, et al., "Small-area bends and beamsplitters for low index-contrast waveguides," *Optics Express*, vol. 11, p. 282, Feb. 2003.
- [3] T. Komljenovic, et al., "Heterogeneous Silicon Photonic Integrated Circuits," *Journal of Lightwave Technology*, vol. 34, pp. 20–35, Jan. 2016.
- [4] S. Han, T. J. Seok, N. Quack, B.-w. Yoo, and M. C. Wu, "Monolithic  $50 \times 50$  MEMS Silicon Photonic Switches with Microsecond Response Time," in *Optical Fiber Communication Conference (2014)*, paper M2K.2, p. M2K.2, Optical Society of America, Mar. 2014.
- [5] P. Edinger, et al., "Compact low loss MEMS phase shifters for scalable field-programmable silicon photonics," *Conference on Lasers and Electro-Optics*, 2020.
- [6] H. Sattari et al., "Silicon Photonic MEMS Add-Drop Filter," 2020 European Conference on Optical Communications (ECOC), 2020.
- [7] W. Bogaerts, et al. Programmable photonic circuits. *Nature* 586, 207–216, 2020.
- [8] H. Sattari et al., "Compact broadband suspended silicon photonic directional coupler," *Opt. Lett.* 45, 2997-3000, 2020.
- [9] A. Y. Takabayashi, et al., "Continuously Tunable Silicon Photonic MEMS  $2 \times 2$  Power Coupler," 2021 21st International Conference on Solid-State Sensors, Actuators and Microsystems (Transducers), pp. 447–450, June 2021.
- [10] A. Y. Takabayashi, et al., "Broadband Compact Single-Pole Double-Throw Silicon Photonic MEMS Switch," *Journal of Microelectromechanical Systems*, vol. 30, pp. 322–329, Apr. 2021.

## CONTACT

\*A. Takabayashi, tel: +41 21 693 77 37;  
[alain.takabayashi@epfl.ch](mailto:alain.takabayashi@epfl.ch)

# Thursday, 13 January

All times are Japanese Standard Time (JST).

## Virtual Poster Session VI and Virtual Exhibit Inspection

**05:00 – 06:30** Presentations are listed by topic category with their assigned number starting on page 36.

## Session XII - Actuators and Switches

Chairs:

Satoshi Konishi, *Ritsumeikan University, JAPAN*

Yukio Suzuki, *Tohoku University, JAPAN*

- 09:15** **COMPACT INTEGRATED SILICON PHOTONIC MEMS POWER COUPLER FOR PROGRAMMABLE PHOTONICS**  
Alain Y. Takabayashi<sup>1</sup>, Duarte Silva<sup>1</sup>, Hamed Sattari<sup>1</sup>, Pierre Edinger<sup>2</sup>, Peter Verheyen<sup>3</sup>, Kristinn B. Gylfason<sup>2</sup>, Wim Bogaerts<sup>4</sup>, and Niels Quack<sup>1,5</sup>  
<sup>1</sup>*École Polytechnique Fédérale de Lausanne (EPFL), SWITZERLAND*, <sup>2</sup>*KTH Royal Institute of Technology, SWEDEN*, <sup>3</sup>*Interuniversity Microelectronics Centre (IMEC), BELGIUM*, <sup>4</sup>*Ghent University, BELGIUM*, and <sup>5</sup>*University of Sydney, AUSTRALIA*
- 09:30** **PHOTOCONDUCTIVE SWITCHING OF A HIGH-VOLTAGE ACTUATOR ARRAY**  
Vesna Bacheva<sup>1,2</sup>, Edouard Leroy<sup>3</sup>, Shai Shumlevich<sup>3</sup>, Aiste Balciunaite<sup>1</sup>, Diana Dávila<sup>1</sup>, Eleonore Cauquil<sup>1</sup>, Israel Gabay<sup>2</sup>, Iago Pereiro<sup>1</sup>, Herbert Shea<sup>3</sup>, Govind V. Kaigala<sup>1</sup>, and Moran Bercovici<sup>2</sup>  
<sup>1</sup>*IBM Research Europe - Zurich, SWITZERLAND*, <sup>2</sup>*Technion - Israel Institute of Technology, ISRAEL*, and <sup>3</sup>*École Polytechnique Fédérale de Lausanne (EPFL), SWITZERLAND*
- 09:45** **A MEMS CONTACTLESS ROTATING TERAHERTZ WAVEGUIDE SWITCH**  
Sofia Rahiminejad, Sven van Berkel, Robin H. Lin, Cecile Jung-Kubiak, Goutam Chattopadhyay, and Mina Rais-Zadeh  
*California Institute of Technology, USA*
- 10:00** **IN-SITU INTEGRATED MICROROBOTS ON A CHIP POWERED BY BIOMOLECULAR ARTIFICIAL MUSCLE**  
Yingzhe Wang<sup>1</sup>, Yuichi Hiratsuka<sup>2</sup>, Takahiro Nitta<sup>3</sup>, and Keisuke Morishima<sup>1</sup>  
<sup>1</sup>*Osaka University, JAPAN*, <sup>2</sup>*Japan Advanced Institute of Science and Technology (JAIST), JAPAN* and <sup>3</sup>*Gifu University, JAPAN*
- 10:15** **SELF-SUSTAINING PNEUMATIC MICRO ACTUATOR FOR LARGE DEFORMATION AND 3D MORPHOLOGY**  
Fade Hu, Xiayu Wang, and Chuan Luo  
*Tsinghua University, CHINA*
- 10:30** **MICRO MAGNETIC PATTERNING ON EXTREMELY TOUGH MAGNETIC GEL ACTUATOR**  
Koichi Ninomiya, Suparat Gaysornkaew, and Fujio Tsumori  
*Kyushu University, JAPAN*

visit us online at \*  
[IEEEMEMS2022.ORG](http://IEEEMEMS2022.ORG)

THE 35TH IEEE INTERNATIONAL CONFERENCE ON MICRO ELECTRO MECHANICAL SYSTEMS



# MEMS 2022

## TOKYO JAPAN

HYBRID

9-13 JANUARY, 2022

# FINAL PROGRAM

CONFERENCE CHAIRS

**Zhihong Li**

Peking University, CHINA

**Shuji Tanaka**

Tohoku University, JAPAN

All indicated times in the program  
are Japan Standard Time (JST)  
The Executive Committee reserves the  
right to amend the program if necessary.



SPONSORED BY



**IEEE**

**MEMS**

IEEE MEMS TECHNOLOGY COMPANY